Article
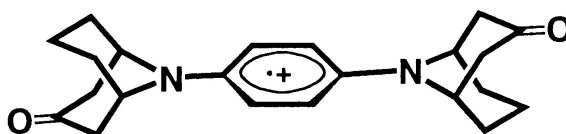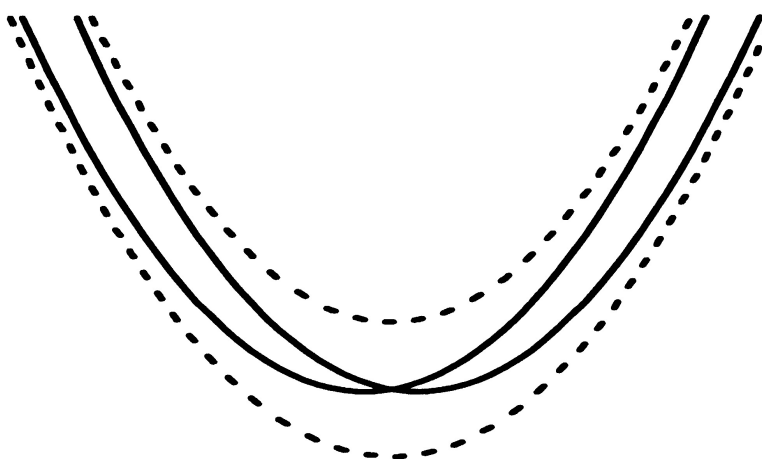
Contributions of Symmetric and Asymmetric Normal Coordinates to the Intervalence Electronic Absorption and Resonance Raman Spectra of a Strongly Coupled *p*-Phenylenediamine Radical Cation

Susan E. Bailey, Jeffrey I. Zink, and Stephen F. Nelsen

More About This Article

Additional resources and features associated with this article are available within the HTML version:

- Supporting Information
- Links to the 10 articles that cite this article, as of the time of this article download
- Access to high resolution figures
- Links to articles and content related to this article
- Copyright permission to reproduce figures and/or text from this article

View the Full Text HTML

Contributions of Symmetric and Asymmetric Normal Coordinates to the Intervalence Electronic Absorption and Resonance Raman Spectra of a Strongly Coupled *p*-Phenylenediamine Radical Cation

Susan E. Bailey,[†] Jeffrey I. Zink,*,[†] and Stephen F. Nelsen*,[‡]

Contribution from the Department of Chemistry and Biochemistry, University of California, Los Angeles, California 90095 and Department of Chemistry, University of Wisconsin, 1101 University Avenue, Madison, Wisconsin 53706-1396

Received November 7, 2002; E-mail: zink@chem.ucla.edu

Abstract: Resonance Raman spectroscopy, electronic absorption spectroscopy, and the time-dependent theory of spectroscopy are used to analyze the intervalence electron transfer properties of a strongly delocalized class III molecule, the tetraalkyl-*p*-phenylene diamine radical cation bis(3-oxo-9-azabicyclo-[3.3.1]non-9-yl)benzene (**(k33)₂PD**⁺). This molecule is a prototypical system for strongly coupled organic intervalence electron transfer spectroscopy. Resonance Raman excitation profiles in resonance with the lowest energy absorption band are measured. The normal modes of vibration that are most strongly coupled to the intervalence transition are identified and assigned by using UB3LYP/6-31G(d) calculations. Excited state distortions are obtained, and the resonance Raman intensities and excitation profiles are calculated by using the time-dependent theory of Raman spectroscopy. The most highly distorted normal modes are all totally symmetric, but intervalence electron transfer absorption spectra are usually interpreted in terms of a model based on coupling between potential surfaces that are displaced along an asymmetric normal coordinate. This model provides a convenient physical picture for the intervalence compound, but it is inadequate for explaining the spectra. The absorption spectrum arising from only the strongly coupled surfaces consists of a single narrow band, in contrast to the broad, vibronically structured experimental spectrum. The electronic absorption spectrum of **(k33)₂PD**⁺ is calculated by using exactly the same potential surfaces as those used for the Raman calculations. The importance of symmetric normal coordinates, in addition to the asymmetric coordinate, is discussed. The observed vibronic structure is an example of the missing mode effect; the spacing is interpreted in terms of the time-dependent overlaps in the time domain.

Introduction

The concept of intervalence (*IV*) compounds was developed in the 1960s for transition metal coordination compounds. The simplest *IV* compounds consist of two identical charge-bearing units **M** (originally metal coordination complexes) that are connected by a divalent ligand **B** that acts as a bridge between the **M** units. If the metals have the same charge at one oxidation level, removal of an electron produces a *IV* compound that may be symbolized as $[\mathbf{M}-\mathbf{B}-\mathbf{M}]^+$ if the **M** units are neutral before electron removal, as they are in the cases we wish to consider. Robin and Day classified *IV* compounds in 1967[1] by considering how large the electronic coupling between the **M** units (which we will call H_{ab}) is relative to the vertical reorganization energy, the amount the energy is increased if an electron is transferred between the **M** groups of a localized *IV* compound without allowing any relaxation, which we will call λ. Robin and Day class I compounds have no electronic interaction between the **M** groups and are not of interest here. Class II compounds have

a small electronic interaction, and their **M** groups are at different oxidation levels, so they may be symbolized $^0\mathbf{M}-\mathbf{B}-\mathbf{M}^+$. Class III compounds have such a large H_{ab} relative to λ that they are delocalized, so they may be symbolized $^{1/2+}\mathbf{M}-\mathbf{B}-\mathbf{M}^{1/2+}$. Thus, $^0\mathbf{M}-\mathbf{B}-\mathbf{M}^+$ and $^+\mathbf{M}-\mathbf{B}-\mathbf{M}^0$ are related by an electron transfer between the **M** groups for class II compounds but are resonance structures for class III compounds. Also in 1967,[2] Hush pointed out that strongly trapped class II intervalence compounds, characterized by having $H_{ab} \ll \lambda/2$, have a featureless, nearly Gaussian-shaped charge transfer band having a transition energy at the band maximum (E_{op} (cm⁻¹) = $10^7/\lambda_{max}$ (nm), where λ_{max} is the wavelength at the band maximum) that is equal to λ, and a bandwidth at half-height of least $(16RT \ln(2)E_{op})^{1/2}$.[2,3] Class II intervalence compounds are the simplest electron transfer systems ever devised, because they have the driving force for electron transfer fixed at $\Delta G_0 = 0$, and the bridge controls distance and relative geometry of the **M** units.[2-5] Hush also pointed out that the transition dipole moment μ_{12} can be

[†] University of California, Los Angeles.
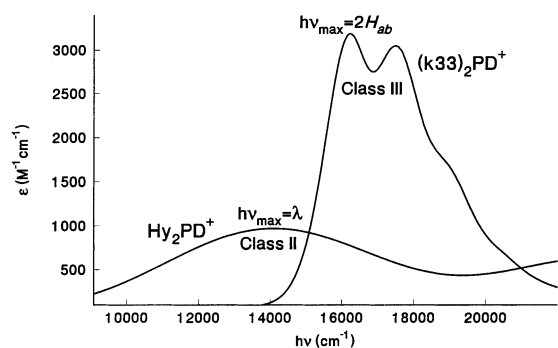[‡] University of Wisconsin, Madison.

(1) Robin, M.; Day, P. *Adv. Inorg. Radiochem.* **1967**, *10*, 247.

(2) Hush, N. S. *Prog. Inorg. Chem.* **1967**, *8*, 391.
(3) Hush, N. S. *Coord. Chem. Rev.* **1985**, *64*, 135.
(4) Marcus, R. A.; Sutin, N. *Biochim. Biophys. Acta* **1985**, *811*, 265.
(5) Sutin, N. *Prog. Inorg. Chem.* **1983**, *30*, 441.

Figure 1. Comparison of the intervalence band absorption spectra of the localized class II **Hy₂PD⁺** and the class III **(k33)₂PD⁺**.

used to estimate the size of H_{ab} in a simple manner. In contrast, strongly delocalized class III compounds (those which have $H_{ab} \gg \lambda/2$) have lowest energy absorption bands that are much narrower and often show vibrational fine structure.

Class II intervalence radical cations with organic **M** groups have charge transfer bands resembling those of transition-metal-centered examples, and Nelsen and co-workers have shown that for some hydrazine- and diazene-centered examples having both saturated and unsaturated bridges, classical two-state Marcus–Hush theory analysis of their charge transfer absorption spectra predicts surprisingly accurately the thermal rate constants for intramolecular electron transfer that were measured by ESR.[6–9] The appearance of the longest wavelength band in the optical absorption spectra for class II and III *IV* compounds can be quite different, as shown for the strongly charged localized class II *p*-phenylene (**PH**)-bridged bis-hydrazine **Hy₂PD⁺** and the strongly delocalized class III tetraalkyl-*p*-phenylene-diamine (**PD**) derivative **(k33)₂PD⁺** in Figure 1.
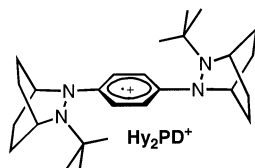
Hy₂PD⁺

The large difference in appearance of the spectra in Figure 1 arises from H_{ab}/λ being very much larger for **(k33)₂PD⁺** than for **Hy₂PD⁺**. The electronic coupling for the latter is only about one-third that of **(k33)₂PD⁺**, because H_{ab} depends on overlaps at the CN bonds that connect the charge-bearing units to the bridge. The **Hy** groups are more twisted (H_{ab} is approximately proportional to the cosine of the twist angle at each N–Ar bond), and the nitrogen attached to the bridge of the **Hy⁺** group only bears about half the charge on the **Hy⁺** unit. Furthermore, λ, which is principally determined by the size of the change in geometry at the charge-bearing units upon electron transfer, is much larger for a hydrazine than for an amine.

Nelsen and co-workers pointed out that double Michael addition of compounds containing amino groups, such as those of *p*-phenylenediamine (**1**, **PD**), to 2,7-cyclooctadieneone (**2**) provides powerful kinetic protection for higher oxidation levels

by converting the NH₂ groups to NR₂ groups that lack removable α-hydrogens.[10] These 3-oxa-9-azabicyclo[3.3.1]nonyl groups will be abbreviated as **(k33)N** groups here, as we have previously when we used **3** and related compounds in intermolecular electron transfer studies.[11]

1 PD   **2**   **3 (k33)₂PD**
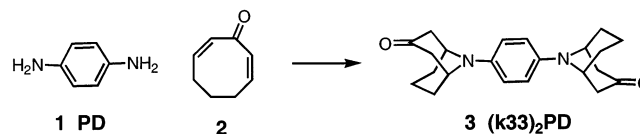
The doubly α-branched alkyl groups required for long lifetime of typical amino-substituted organic radical cations cause thermodynamically easier oxidation than do smaller alkyl groups because they provide better electron delocalization than do α-unbranched alkyl groups, but the presence of the keto group at the 3 position of the **(k33)N** substituents of **3** has been shown to result in a very similar stabilization to the positive charge of **3⁺** and electronic coupling as the dimethylamino groups of the tetramethyl-*p*-phenylenediamine radical cation (**TMPD⁺**).[12] The radical cations of **PD** derivatives are exceptionally stable and do not require such kinetic protection; they were in fact the first organic radical cations ever prepared.[13] Our current interest in these compounds is as organic intervalence compounds, for which the kinetic protection supplied by **(k33)N** groups is required in less stable examples than **3⁺**.

Scheme 1. Adiabatic and Diabatic Structures for PD⁺

Adiabatic **PD⁺**

Diabatic models for **PD⁺**
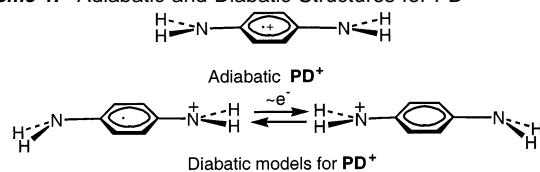
The present work is concerned with time-dependent theoretical analysis[14] of aryl-bridged intervalence compounds that have **(k33)N** as the **M** units, specifically the strongly delocalized class III **3⁺** (**(k33)₂PD⁺**). As indicated in Scheme 1, the geometries would be significantly different for geometry-relaxed delocalized **PD⁺** and its derivatives, which lie on the adiabatic surface, that is, with the large electronic coupling intact, and for the starting point of a two-state analysis, the pair of hypothetical diabatic structures that would be present if H_{ab} was zero.

The electronic absorption spectrum and the resonance Raman spectrum of intervalence compounds are frequently interpreted by using potential energy surfaces such as those shown in Figure 2. The solid lines illustrate diabatic surfaces, one of which represents the molecule with the charge on the right, the other with the charge on the left. The dotted lines represent the ground and vertical excited-state adiabatic surfaces for an $H_{ab} \gg \lambda/2$ case like **(k33)₂PD⁺**.

The potential energy surfaces in Figure 2 provide a convenient physical picture for the intervalence compound, but they are

(6) Nelsen, S. F.; Ismagilov, R. F.; Trieber, D. A. I. *Science* **1997**, *278*, 846.
(7) Nelsen, S. F.; Ismagilov, R. F.; Powell, D. R. *J. Am. Chem. Soc.* **1997**, *119*, 10213.
(8) Nelsen, S. F.; Ismagilov, R. F.; Gentile, K. E.; Powell, D. R. *J. Am. Chem. Soc.* **1999**, *121*, 7108.
(9) Nelsen, S. F.; Trieber, D. A. I.; Ismagilov, R. F.; Teki, Y. *J. Am. Chem. Soc.* **2001**, *123*, 5684.

(10) Nelsen, S. F.; Kessel, C. R.; Brien, D. J. *J. Am. Chem. Soc.* **1980**, *102*, 2, 702.
(11) Nelsen, S. F.; Pladziewicz, J. R. *Acc. Chem. Res.* **2002**, *35*, 247 and references therein.
(12) Nelsen, S. F.; Tran, H. Q.; Nagy, M. A. *J. Am. Chem. Soc.* **1998**, *120*, 298.
(13) Roth, H. D. *Tetrahedron* **1986**, *42*, 5097, for the early history of radical ion studies.
(14) Zink, J. I.; Shin, K.-S. K. In *Advances in Photochemistry*; Wiley: New York, 1991; Vol. 16, p 119.
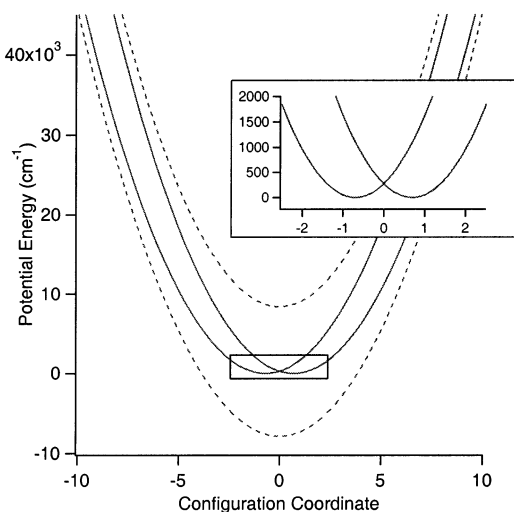
Figure 2. Asymmetric cross section of the ten-dimensional potential energy surface used to fit the absorption spectrum of $(k33)_2PD^+$; the dotted lines illustrate the adiabatic surfaces (frequency of 1090 cm^{-1}), the solid lines illustrate the diabatic surfaces (frequency of 1110 cm^{-1} and distortions of +0.7 and -0.7, respectively), and the inset magnifies the crossing point for the diabatic surfaces.
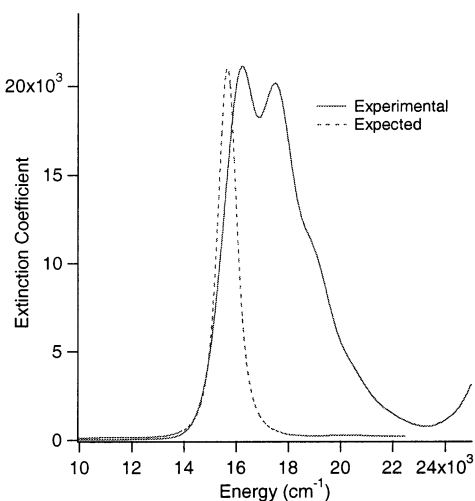
Figure 3. Absorption spectrum of $(k33)_2PD^+$ in acetonitrile in the intervalence region (solid line) and the calculated spectrum for the interacting diabatic surfaces shown in Figure 2 (dotted line).

inadequate for explaining the spectra. For example, the absorption spectrum arising from the strongly coupled surfaces depicted in Figure 2 consists of a single narrow band, in contrast to the vibronically structured spectrum in Figure 1. An example of the spectrum arising from the coupled surfaces, to be discussed in detail in this paper, is shown in Figure 3.

The depiction of an intervalence absorption band in terms of one configuration coordinate representing structures such as those in Scheme 1 needs to be expanded because the actual motions of large molecules that display intervalence electron transfer spectra will be distributed over a number of coordinates, both symmetric and asymmetric. The necessity of including the symmetric normal modes is well recognized from both a theoretical[15-21] and experimental point of view.[22-35] The

majority of the experimental work involved mixed valence inorganic molecules consisting of two metals in different formal oxidation states separated by a bridging ligand,[15-19,22-35] but recent studies have been carried out on organic molecules including triarylamine mixed valence systems.[20,21]

In this paper, we use resonance Raman spectroscopy, electronic absorption spectroscopy, and the time-dependent theory of spectroscopy to analyze the properties of $(k33)_2PD^+$. Resonance Raman excitation profiles in resonance with the lowest energy absorption band are measured. The normal modes of vibration that are most strongly coupled to the transition are identified and assigned by using Gaussian 98 calculations. All of the resonance Raman intensities and excitation profiles are calculated by using the time-dependent theory, and the excited state distortions are obtained. The methods for calculating the Raman and electronic absorption spectra for models of intervalence electron transfer such as the surfaces in Figure 2 are discussed, and the spectra are calculated and interpreted. The electronic absorption spectrum is calculated by using exactly the same potential surfaces as those used for the Raman calculations. The importance of symmetric normal coordinates, in addition to the asymmetric coordinate depicted in Figure 2, is discussed. The vibronic structure is an example of the missing mode effect;[36-39] the spacings are interpreted in terms of the time-dependent overlaps in the time domain. The $(k33)_2PD^+$ molecule is a prototypical system for strongly coupled organic intervalence electron transfer spectroscopy.

Experimental Section

Neutral $(k33)_2PD$ was prepared as previously described,[10] oxidized to the radical cation hexafluorophosphate salt $(k33)_2PD^+PF_6^-$ using NOPF$_6$, and characterized by X-ray crystallography.[40] The absorption spectrum of $(k33)_2PD^+PF_6^-$ in acetonitrile was recorded at room temperature on a Perkin-Elmer Lambda 20 absorption spectraphotometer.[41]

Vibrational Spectroscopy. Raman spectra were collected by a double monochromator and detected with a PMT or collected by a triple

(15) Piepho, S. B. *J. Am. Chem. Soc.* **1988**, *110*, 6319.
(16) Piepho, S. B. *J. Am. Chem. Soc.* **1990**, *112*, 4197.
(17) Reimers, J. R.; Hush, N. S. *Chem. Phys.* **1996**, *208*, 177.
(18) Hush, N. S. *NATO Adv. Study Inst. Ser., Ser. C* **1980**, *58*, 151.
(19) Talaga, D. S.; Zink, J. I. *J. Phys. Chem. A* **2001**, *105*, 10511.
(20) Coropceanu, V.; Malagoli, M.; Andre, J. M.; Bredas, J. L. *J. Chem. Phys.* **2001**, *115*, 10409.
(21) Coropceanu, V.; Malagoli, M.; Andre, J. M.; Bredas, J. L. *J. Am. Chem. Soc.* **2002**, *124*, 10519.
(22) Dong, Y. H.; Hupp, J. T.; Yoon, D. I. *J. Am. Chem. Soc.* **1993**, *115*, 4379.
(23) Hupp, J. T.; Dong, Y. H. *Inorg. Chem.* **1994**, *33*, 4421.
(24) Petrov, V.; Hupp, J. T.; Mottley, C.; Mann, L. C. *J. Am. Chem. Soc.* **1994**, *116*, 2171.
(25) Roberts, J. A.; Hupp, J. T. *Inorg. Chem.* **1992**, *31*, 157.
(26) Demadis, K. D.; El-Samanody, E.-S.; Coia, G. M.; Meyer, T. J. *J. Am. Chem. Soc.* **1999**, *121*, 535.
(27) Demadis, K. D.; Neyhart, G. A.; Kober, E. M.; White, P. S.; Meyer, T. J. *Inorg. Chem.* **1999**, *38*, 5948.
(28) Hornung, F. M.; Baumann, F.; Kaim, W.; Olabe, J. A.; Slep, L. D.; Fiedler, J. *Inorg. Chem.* **1998**, *37*, 311.
(29) Williams, R. D.; Petrov, V. I.; Lu, H. P.; Hupp, J. T. *J. Phys. Chem. A* **1997**, *101*, 8070.
(30) Karki, L.; Williams, R. D.; Hupp, J. T.; Allan, C. B.; Spreer, L. O. *Inorg. Chem.* **1998**, *37*, 2837.
(31) Lu, H.; Petrov, V.; Hupp, J. T. *Chem. Phys. Lett.* **1995**, *235*, 521.
(32) Ko, J.; Ondrechen, M. J. *Chem. Phys. Lett.* **1984**, *112*, 507.
(33) Ondrechen, M. J.; Ko, J.; Root, L. J. *J. Phys. Chem.* **1984**, *88*, 5919.
(34) Ondrechen, M. J.; Ferretti, A.; Lami, A.; Villani, G. *J. Phys. Chem.* **1994**, *98*, 11230.
(35) Ferretti, A.; Lami, A.; Ondrechen, M. J.; Villani, G. *J. Phys. Chem.* **1995**, *99*, 10484.
(36) Tutt, L.; Tannor, D.; Heller, E. J.; Zink, J. I. *Inorg. Chem.* **1982**, *21*, 1, 3858.
(37) Tutt, L.; Tannor, D.; Schindler, J.; Heller, E. J.; Zink, J. I. *J. Phys. Chem.* **1983**, *87*, 3017.
(38) Tutt, L.; Zink, J. I. *J. Am. Chem. Soc.* **1986**, *108*, 5830.
(39) Tutt, L.; Zink, J. I.; Heller, E. J. *Inorg. Chem.* **1987**, *26*, 2158.
(40) Nelsen, S. F.; Ramm, M. T.; Ismagilov, R. F.; Nagy, M. A.; Trieber, D. A. I.; Powell, D. R.; Chen, X.; Gengler, J. J.; Qu, Q.; Brandt, J. L.; Pladziewicz, J. R. *J. Am. Chem. Soc.* **1997**, *119*, 5900.
(41) Nelsen, S. F.; Tran, H. Q. *J. Phys. Chem. A* **1999**, *103*, 8139.

monochromator and detected by a CCD. Excitation was provided by an argon ion laser (for wavelengths of 514.5, 488, and 457 nm) and Krypton ion laser (for wavelengths of 568, and 676 nm). An interference filter was used with 488 and 457 nm excitations to eliminate plasma lines.

Spectra were collected from spinning pellets made from a finely ground mixture of (k33)$_2$PD$^+$ and the reference compound KNO$_3$ at a ratio of 1:28 in KCl. The intensities were obtained by numerically integrating the peaks. The Raman intensities were normalized to that of the KNO$_3$ standard. Spectra were collected in triplicate; averages and standard deviations are reported. The plot of the normalized intensity versus the energy of excitation is a resonance Raman profile.

Theoretical Methods

The theoretical foundation underlying the calculation of spectra for coupled and uncoupled potential surfaces in the framework of the time-dependent theory of molecular spectroscopy is briefly presented in this section.[42-44] The time-dependent approach is very powerful from both the technical and conceptual points of view. Its utility is particularly evident in the treatment of coupled electronic states; in the time-independent (Franck–Condon) picture, the spectroscopic consequences of coupling between states are much harder to visualize qualitatively and to calculate quantitatively than with time-dependent methods.

Absorption Spectra. The fundamental equation for the calculation of an absorption spectrum in the time-dependent theory is[43,45,46]

$$I(\omega) = C\omega \int_{-\infty}^{+\infty} \exp(i\omega t) \left\{ \langle \Phi | \Phi(t) \rangle \exp\left(-\Gamma t + \frac{iE_0}{h}t \right) \right\} dt \quad (1)$$

with $I(\omega)$ as the absorption intensity at frequency ω, E_0 as the energy of the electronic origin transition, and Γ as a phenomenological damping factor.

The most important ingredient to eq 1 is $\langle \Phi | \Phi(t) \rangle$, the autocorrelation function of the wave packet Φ prepared after the spectroscopic transition. In the absence of coupling terms between the normal coordinates, the total autocorrelation in a system with K coordinates is given by

$$\langle \Phi | \Phi(t) \rangle = \prod_k \langle \phi^k | \phi^k(t) \rangle \quad (2)$$

where ϕ^k is a wave packet associated with coordinate k ($k = 1,..., K$) and is a two-dimensional vector: $\phi^k(Q_k, j)$, where Q_k is the coordinate along mode K and $j = 1,2$ is an index over the two electronic states. In the following, we will eliminate the index k and consider only a single coordinate. The $t = 0$ wave packet is then defined as

$$\phi(t = 0) = \mu\chi_i \quad (3)$$

or more explicitly:

$$\phi(Q,j,t = 0) = \sum_{j'=1}^{2} \mu_{jj'}(Q)\chi_i(Q,j') \, j = 1,2 \quad (4)$$

Here, the subscript "i" denotes the initial state; χ_i is an eigenstate of the combined two-electronic states and the single vibration Hamiltonian (typically the groundstate of the combined two-electronic states and a single vibration Hamiltonian). We do not label ϕ by the initial state index i to avoid cluttering with indices, but the wave packet depends on the initial state. The transition moment μ for coordinate k is formally a 2 by 2 matrix which is coordinate dependent ($\mu_{jj'}(Q)$). It is usually an off-diagonal matrix, and the off-diagonal value is a mode-dependent

and possibly coordinate-dependent value, μ, such that $(\mu)^2$ is proportional to the cross section for absorption in mode k. Thus, in practice,

$$\phi(Q,j = 1,t = 0) = \mu(Q)\chi_i(Q,2)$$

$$\phi(Q,j = 2,t = 0) = \mu(Q)\chi_i(Q,1) \quad (5)$$

For two coupled excited states, we need to keep track of two wave packets, ϕ_1 and ϕ_2, moving on the two coupled potential surfaces.[47-49] The wave packet $\phi(t)$ is given by the time-dependent Schrödinger equation:

$$i\frac{\partial}{\partial t}\begin{pmatrix} \phi_1 \\ \phi_2 \end{pmatrix} = \begin{pmatrix} H_1 & V_{12} \\ V_{21} & H_2 \end{pmatrix}\begin{pmatrix} \phi_1 \\ \phi_2 \end{pmatrix} \quad (6)$$

(where now the subscript denotes the electronic state, $j = 1$ or 2), and the total overlap $\langle \phi | \phi(t) \rangle$ is calculated as

$$\langle \phi | \phi(t) \rangle = \langle \phi_1 | \phi_1(t) \rangle + \langle \phi_2 | \phi_2(t) \rangle \quad (7)$$

The diagonal elements H_j of the total Hamiltonian are given as

$$H_j = -\frac{1}{2M}\nabla^2 + V_j(Q) \quad (8)$$

(where $j = 1,2$), $V_j(Q)$ is the potential energy as a function of the configurational coordinate Q, $-1/2M\cdot\nabla^2$ is the nuclear kinetic energy, and $V_{12} = V_{21}$ is the coupling between the two diabatic potentials. For simplicity, displaced harmonic excited state potentials for the symmetric normal modes are chosen, although the theoretical method is not restricted by the functional form of the potentials. The displacement of the minimum of one electronic state from the other, from that of the ground state, ΔQ, is abbreviated as Δ in this paper. The potentials are given by

$$V_j(Q) = \frac{1}{2}k_j(Q - \Delta Q_j)^2 + E_j \quad (9)$$

with $k_j = 4\pi^2 M(\hbar\omega_j)^2$ as the force constant, $\Delta Q_j (= \pm\Delta)$ as the position of the potential minimum for electronic state j along Q, and E_j as the energy of the potential minimum for state j.

The uncoupled potentials are shown as dashed lines in Figure 2 (diabatic potentials). The coupling between the diabatic potentials for states 1 and 2 is chosen to be coordinate independent in this paper, although the computational method allows us to use coordinate dependent coupling. Note that different authors use the symbols for the coupling V_{12} or H_{ab} or ϵ interchangeably. The symbol H_{ab} is used in the remainder of this paper because it is most commonly found in discussions of organic compounds.

The theoretical treatment of the intervalence band is a special case of the general picture[50-59] because the potential is symmetric and because the spectrum is calculated by propagating the two components of the lowest energy eigenfunctions ($i = 0$) of the coupled system. The appropriate potential surfaces are shown in Figure 2.

The complete one-dimensional picture requires that the lowest energy eigenfunction of the coupled surfaces be calculated. This eigenfunction has two components, one from each of the diabatic surfaces. The

(42) Lee, S.-Y.; Heller, E. J. *J. Chem. Phys.* **1979**, *71*, 4777.
(43) Heller, E. J. *Acc. Chem. Res.* **1981**, *14*, 368.
(44) Heller, E. J.; Sundberg, R. L.; Tannor, D. *J. Phys. Chem.* **1982**, *86*, 1822.
(45) Heller, E. J. *J. Chem. Phys.* **1975**, *62*, 1544.
(46) Heller, E. J. *J. Chem. Phys.* **1978**, *68*, 2066.

(47) Alvarellos, J.; Metiu, H. *J. Chem. Phys.* **1988**, *88*, 4957.
(48) Jiang, X. P.; Heather, R.; Metiu, H. *J. Chem. Phys.* **1989**, *90*, 2555.
(49) Heather, R.; Metiu, H. *J. Chem. Phys.* **1989**, *90*, 6903.
(50) Reber, C.; Zink, J. I. *J. Phys. Chem.* **1992**, *96*, 571.
(51) Reber, C.; Zink, J. I. *J. Chem. Phys.* **1992**, *96*, 2681.
(52) Wexler, D.; Reber, C.; Zink, J. I. *J. Phys. Chem.* **1992**, *96*, 8757.
(53) Simoni, E.; Reber, C.; Talaga, D. S.; Zink, J. I. *J. Phys. Chem.* **1993**, *97*, 12678.
(54) Wexler, D.; Zink, J. I. *Inorg. Chem.* **1995**, *34*, 1500.
(55) Wootton, J. L.; Zink, J. I. *J. Phys. Chem.* **1995**, *99*, 7251.
(56) Talaga, D. S.; Zink, J. I. *J. Phys. Chem.* **1996**, *100*, 8712.
(57) Wootton, J. L.; Zink, J. I. *J. Am. Chem. Soc.* **1997**, *119*, 1895.
(58) Neuhauser, D.; Park, T.-J.; Zink, J. I. *Phys. Rev. Lett.* **2000**, *85*, 5304.
(59) Acosta, A.; Cheon, J.; Zink, J. I. *Inorg. Chem.* **2000**, *39*, 427.

eigenfunction is calculated as follows:

$$\chi_i = \text{const.} \bullet \int_0^T \eta(t)w(t)\exp\!\left(\frac{iE_i}{h}t\right)\!dt \qquad (10)$$

where χ_i denotes the eigenfunction corresponding to the eigenvalue E_i, $\eta(t)$ is the time-dependent (propagating) wave function which initially is located arbitrarily on the surface, and $w(t)$ is a Hanning window function. The initial energy E_i is estimated from plotting the norm of the resulting χ_i as a function of energy; $E_{i=0}$ is the energy of the lowest peak. Note that for coupled potentials, each eigenfunction χ_i is an array with two components corresponding to the two diabatic potentials that form the basis in the calculations; that is, χ_i is specifically $\chi_i(Q,j)$.

There are two major differences from the usual case of noncoupled potential surfaces that involves a lower (ground) and upper (excited) state. First, in the coupled case, the wave packet motion is on both states, while, in the usual case, the wave packet propagates on a single (the excited) state. Second, in the coupled case, the initial wave packet involves the lowest eigenfunction of the coupled system, while, in the usual case, it is the vibrational wave function times the transition dipole from a completely different electronic surface.

The configurational coordinate in Figure 2 requires further explanation. It is rarely defined precisely, in part, because there are usually several possibilities and it is difficult to choose the most important one. The coordinate that is chosen here is an asymmetric ring stretching mode with a vibrational energy of 1090 cm^{-1}.

Raman Spectra. The Raman scattering cross section is given by[60]

$$\alpha_{fi} = \frac{i}{\hbar}\int_0^\infty (\sum_{r=1}^n \mu_r^2 \langle\phi_f|\phi(t)\rangle_r \exp(-iE_{00}^{(r)}t - \Gamma^{(r)}t))\exp\{i(\omega_i+\omega_1)t\}dt \qquad (11)$$

where $|\phi_f\rangle = \mu|\chi_f\rangle$ is the final vibrational state, χ_f, multiplied by the transition electric dipole moment, μ, $|\phi(t)\rangle = \exp(-iH_{ex}t/h)|\phi\rangle$ is a moving wave packet propagated by the Hamiltonian, $|\phi\rangle = \mu|\chi\rangle$ is the initial vibrational state multiplied by the electronic transition moment, Γ is the damping factor, $h\omega_i$ is the zero point energy of the ground electronic surface, and $\hbar\omega_1$ is the energy of the incident radiation. The Raman intensity $I_{i\to f}$ into a particular mode f is

$$I_{i\to f} \approx \omega_1\omega_s^3[\alpha_{fi}]^*[\alpha_{fi}] \qquad (12)$$

where ω_s is the frequency of the scattered radiation.

Results

1. Absorption Spectroscopy. The acetonitrile solution absorption spectrum of **(k33)$_2$PD$^+$** in the visible wavelength region is shown in Figures 1 and 3. The room temperature spectrum contains peaks at 16234 ± 100 cm^{-1} (616 nm) and 17483 ± 100 cm^{-1} (572 nm) and a shoulder at 18832 ± 300 cm^{-1} (531 nm). These features are separated by an average of 1324 cm^{-1}. The band maximum appears at 16200 ± 100 cm^{-1} and has an extinction coefficient of 21000 M^{-1}cm^{-1}.

2. Resonance Raman Spectroscopy. Plots of the integrated Raman intensities as a function of the excitation energy (the resonance Raman excitation profiles) are given in Figure 4. The frequencies (in wavenumbers) and intensities (relative to that of the KNO$_3$ standard peak at 1046 cm^{-1}) obtained for a 568 nm (17605 cm^{-1}) excitation (the wavelength that produces the maximum Raman intensity) are as follows: 194, 1.52; 405, 2.97; 505, 2.19; 819, 0.98; 894, 1.10; 960, 1.12; 1014, 3.47; 1059, 1.51; 1095, 1.68; 1237, 2.82; 1253, 3.01; 1342, 3.07; 1368, 4.25;

(60) Shin, K.-S. K.; Zink, J. I. *Inorg. Chem.* **1989**, *28*, 4358.
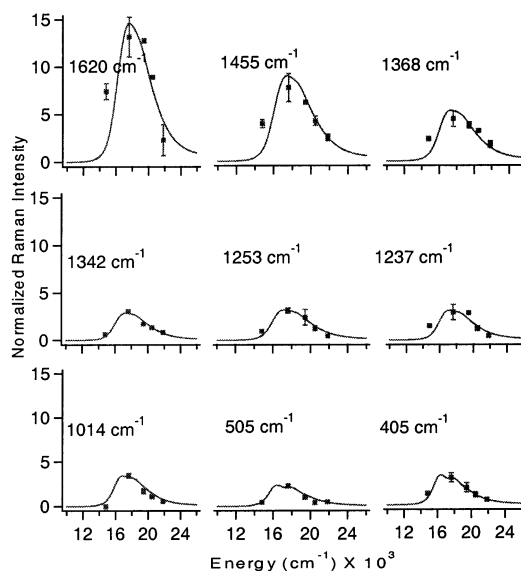
Figure 4. Resonance Raman excitation profiles of the nine most enhanced modes for **(k33)$_2$PD$^+$**. The experimental points are shown with error bars, and the calculated fit is shown as a solid line. Experimental data were collected from solid samples with intensities referenced to KNO$_3$ as the internal standard. All experimental and calculated plots are shown on the same scale.

1455, 7.41; 1513, 0.82; 1620, 13.18; 1799, 3.11. The bands with observed enhancements of at least 10% of that of the most intense band at 1620 cm^{-1} are plotted in Figure 4 with error bars indicating one standard deviation from at least three measurements. The spectra were obtained using 676, 568, 514.5, 488, and 457 nm excitations.

Discussion

1. Absorption Spectrum for Strong Coupling. The electronic absorption spectrum of **(k33)$_2$PD$^+$** shown in Figures 1 and 3 is typical of that measured for strongly coupled, delocalized molecules. The band is narrower than those from molecules with intermediate values of delocalization, and it also exhibits vibronic structure. Based on the energy of the band maximum, the calculated value of the coupling H_{ab} is 8120 cm^{-1}.

Interpretation of the absorption band in terms of a model based on two coupled diabatic potential surfaces such as those shown in Figure 2 reveals an important limitation of the model: the experimental bandwidth is much larger than that predicted by the model. For example, the absorption spectrum calculated by using $H_{ab} = 8120$ cm^{-1} and a vibrational frequency of 1090 cm^{-1} is shown superimposed on the experimental spectrum in Figure 3. The spectrum contains only one peak, not the vibronic progression observed in the experimental spectrum.

The reason that the model depicted in Figure 2 predicts a narrow structure-free absorption spectrum can be understood in terms of the dynamics of the wave packet in the time domain. The width of the spectrum is determined by the initial decrease of the overlap, which in turn is governed by the slope of steepest descent. The steeper the slope, the faster the movement of the wave packet and the broader the spectrum. Vibronic structure is caused by the recurrence of overlap in the time domain. A simple physical picture for the strongly coupled system is obtained by visualizing wave packet motion on the upper

adiabatic surface in Figure 2. The vibrational wave function of the lowest energy surface is multiplied by the transition dipole moment and is propagated on the upper surface. Because of the strong coupling, the minimum of the upper surface is vertically above that of the lower surface. Thus, the center of the wave packet on the upper surface does not move, and the overlap does not change very much as a function of time. The overlap would not change at all if the curvatures of the two surfaces were the same (i.e., if the force constants were the same), and thus, the spectrum would consist of a single sharp line. Because the curvatures are different, the overlap does change slightly, but the majority of the absorbance is contained in the single line, as shown in Figure 3. It is important to emphasize that the calculated spectrum is exact within the framework of the model and is not carried out in the adiabatic limit, but thinking in terms of the adiabatic Born–Oppenheimer surface is useful in understanding the result.

The resonance Raman results prove that other vibrational normal modes play a role in the electronic transition and thus will contribute to the bandwidth. The contribution of these normal modes, especially symmetric modes where potential surfaces are displaced, wave packet motions are large, and large overlap changes occur in the time domain, is discussed in the next section.

2. Involvement of Symmetric Normal Modes Determined by Resonance Raman Spectroscopy. Absorption bands with large widths result when excited state potential surfaces have large displacements relative to the ground state. These displacements, caused by changes in the bond lengths and bond angles, result in nonzero slopes of the excited state potential surface in the Franck–Condon region, cause rapid decreases of the overlap in the time domain, and thus produce a large spread in the frequency domain.

Resonance Raman spectra and excitation profiles, taken at resonance with the excited electronic state of interest, are used to determine the magnitude of the distortion of the mode that is being measured in the profile. Because each normal mode is examined individually, the distortions along each of the normal modes can be calculated. Whereas the electronic spectrum contains information about all of the modes simultaneously, the resonance Raman profile filters out the detailed information about the excited state potential surface along that normal coordinate.

The resonance Raman excitation profiles are plots of resonance Raman intensities of a given mode as a function of excitation wavelengths. (The more familiar Raman spectrum is a plot of the intensities of the modes versus their vibrational frequencies at a specific excitation wavelength.) The width of an excitation profile is determined by the total displacements of all the vibrational modes displaced in the excited state the same way as that of the absorption and emission spectra. It thus contains information about the distortions of all of the normal modes. However, each individual vibrational mode has its own intensity and excitation profile. Therefore, each normal mode's profile contains the information about that specific mode, and the distortions can be obtained from the relative intensities of the excitation profiles.

The purpose of this section is to discuss how resonance Raman spectroscopy is used to determine which normal modes, in addition to the asymmetric mode shown in Figure 2, are

displaced in the excited electronic state. The time-dependent theory is used to calculate the profiles and spectra and to quantify the most important excited state distortions. The discussion focuses on the normal modes whose resonance Raman intensities are 10% or greater than that of the most intense band at 1620 cm^{-1}.

2.1. Assignments of Vibrations. A UB3LYP/6-31G(d) geometry optimization[61] of **(k33)$_2$PD$^+$** gave a nearly pure doublet ($\langle S^2 \rangle = 0.760$) C$_1$ structure having a quinonoid-like distortion of the benzene ring: CN distances, 1.361 Å; NC–CH distances, 1.431 Å; and HC–CH distances, 1.371 Å. The nitrogens are planar, and there is a 16.4° twist angle between the aromatic ring and the N(C)$_2$ planes. The dipole moment components are −0.02, +0.07, and +0.93 D, and this structure is a minimum, with no imaginary vibrational frequencies.[62] The nine strongest observed resonance Raman frequencies are compared with those arising from this calculation in Table 1. The assignments cannot be considered certain for the lower Δ bands in the center of Table 1.

The most intense mode in the resonance Raman spectra is the symmetric aromatic CC and CN stretch that is observed at 1620 cm^{-1} and calculated (after including the correction factor of 0.982 which gave the best fit to the experimental spectrum for the tetramethyl compound)[63] at 1646 cm^{-1}. The largest motions of atoms in the aromatic core of the molecule are shown in cartoon form in Scheme 2. In this strongly coupled (high H_{ab}) molecule, the adiabatic potential surfaces are a good approximation and the electronic transition can be thought of as a bonding orbital to antibonding orbital transition. This transition will weaken CC and CN bonds resulting in an excited state potential surface that is displaced along the symmetric normal mode involving these atoms. Wave packet motion in this coordinate will lead to enhanced resonance Raman intensity. The most highly distorted normal coordinate is the out of plane R$_2$NArNR$_2$ bend at 405 cm^{-1}. The motion involves a large amplitude phenyl ring tilt, maintains the C$_i$ point group, and is a totally symmetric Ar–N bending vibration. The measured resonance Raman intensity of this mode is much smaller than that of the 1620 cm^{-1} mode, but its distortion is larger because the distortion scales as the square root of the intensity and the inverse square of the frequency.

2.2. Calculation of the Experimentally Determined Resonance Raman Intensities and Excitation Profiles. The intensities of the resonance Raman bands and the excitation profiles are calculated by using eqs 9 and 10. The variable parameters that are used in the calculation are the damping Γ and the distortions. For each normal coordinate, its frequency, ω, and

(61) Frisch, M. J.; Trucks, G. W.; Schlegel, H. B.; Scuseria, G. E.; Robb, M. A.; Cheeseman, J. R.; Zakrzewski, V. G.; Montgomery, J. A. J.; Stratmann, R. E.; Burant, J. C.; Dapprich, S.; Millam, J. M.; Daniels, A. D.; Kudin, K. N.; Strain, M. C.; Farkas, O.; Tomasi, J.; Barone, V.; Cossi, M.; Cammi, R.; Mennucci, B.; Pomelli, C.; Adamo, C.; Clifford, S.; Ochterski, J.; Petersson, G. A.; Ayala, P. Y.; Cui, Q.; Morokuma, K.; Malick, D. K.; Rabuck, A. D.; Raghavachari, K.; Foresman, J. B.; Cioslowski, J.; Ortiz, J. V.; Baboul, A. G.; Stefanov, B. B.; Liu, G.; Liashenko, A.; Piskorz, P.; Komaromi, I.; Gomperts, R.; Martin, R. L.; Fox, D. J.; Keith, T.; Al-Laham, M. A.; Peng, C. Y.; Nanayakkara, A.; Gonzalez, C.; Challacombe, M.; Gill, P. M. W.; Johnson, B.; Chen, W.; Wong, M. W.; Andres, J. L.; Gonzalez, C.; Head-Gordon, M.; Replogle, E. S.; Pople, J. A. *Gaussian 98*, revision A.7; Gaussian, Inc.: Pittsburgh, PA, 1998.
(62) The structure was recalculated imposing C$_i$ symmetry using Spartan '02 PC/x86 release 115b, and although the enthalpy decreased 0.76 kcal/mol, the frequencies calculated for all of the vibrations differed by 1.2 cm^{-1} or less from those of the structure calculated without imposing symmetry. We use the Gaussian calculation, for which Raman intensities are available.
(63) Brouwer, A. M. *J. Phys. Chem. A* **1997**, *101*, 3626.

Table 1. Raman Frequencies, Distortions, Reorganization Energies, and Assignments

frequency (cm^{-1})	relative intensity	dimensionless distortion	reorganization energy[a] (cm^{-1})	calculated frequency[b] (cm^{-1})	assignment
405	22.5	1.0710	232	405	out of plane R$_2$NArNR$_2$ bend (large amplitude phenyl ring tilt)
505	16.6	0.7242	132	521	out of plane R$_2$NArNR$_2$ bend (large amplitude N displacement)
1014	26.3	0.4692	111.6	1015	in plane Ar ring breathing
1237	21.4	0.3672	83.39	1220	C−C stretching on k33
1253	22.8	0.3672	84.48	1246	C−H wagging
1342	23.3	0.3366	76.03	1342	N−Ar and Ar C−C stretching
1368	32.2	0.4386	131.6	1363	N−Ar−N in plane stretch
1455	56.2	0.5406	212.6	1463	N−Ar−N in plane stretch
1620	100.0	0.6426	334.5	1646	Ar C=C and N−Ar−N stretches

[a] The reorganization energy, λ, equals $0.5k\delta^2$. The distortion, δ, in units of Å equals 5.807 times the dimensionless distortion times the reciprocal square root of the mass and times the reciprocal square root of the frequency. The force constant, k, in units of cm^{-1}/Å^2 equals 0.02966 times the mass times the frequency squared. [b] The UB3LYP/6-31G(d) calculated mode times the 0.982 factor that Brouwer[63] found led to the best agreement for the tetramethyl compound.

Scheme 2. Largest Motions for the Largest Intensity and Highest Distortion Resonance Raman Bands Observed


1620 cm^{-1} mode   405 cm^{-1} mode
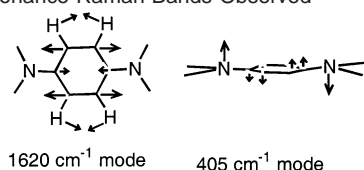
distortion, Δ, define the potential energy surface (eq 5). Wave packet propagation on the ten-dimensional surface (eq 4) determines $\phi(t)$, and the resonance Raman excitation profiles are calculated using $\phi(t)$ according to eqs 9 and 10. (The intensity of each excitation profile in Figure 4 is roughly proportional to $\omega^2\Delta^2$.) The same potential energy surfaces (and thus the same $\phi(t)$) are used to calculate the absorption spectrum (eq 1). Only one set of parameters is used to calculate all of the excitation profiles, to calculate the resonance Raman spectrum at a given excitation wavelength, and to calculate the absorption spectrum as discussed in section 4. The nine spectra were fit simultaneously using the distortions shown in Table 1 and $\Gamma = 1300$ cm^{-1}.

3. Calculation of the Resonance Raman Intensities and Excitation Profiles of Asymmetric Modes Involved in Intervalence Electron Transfer. The intensities of asymmetric normal modes in the resonance Raman spectra, specifically that of the mode depicted in Figure 2, are small. The most intense peaks in the resonance Raman spectra arise from displaced symmetric normal modes. The relative intensities are related to the overlap of the ground state eigenfunction propagated on the excited state surface and the first vibrational excited state on the ground surface. The larger the displacement, the faster the increase in the overlap and the more intense the peak in the spectrum.

The potential surfaces in Figure 2 represent an asymmetric mode with a vibrational frequency of 1090 cm^{-1}. Gaussian calculations assign the 1090 cm^{-1} mode as an asymmetric CN stretch. Experimentally, an intense band is observed in the IR spectrum at 1099 cm^{-1}, and a weak Raman feature is observed at 1095 cm^{-1}; the relative intensities are consistent with an asymmetric vibration in the point group of this molecule. The diabatic surfaces are constructed with a frequency of 1110 cm^{-1} and the distortions $+0.7$ and -0.7, respectively. The coupling of 8120 cm^{-1} was determined by previous analysis.[12]
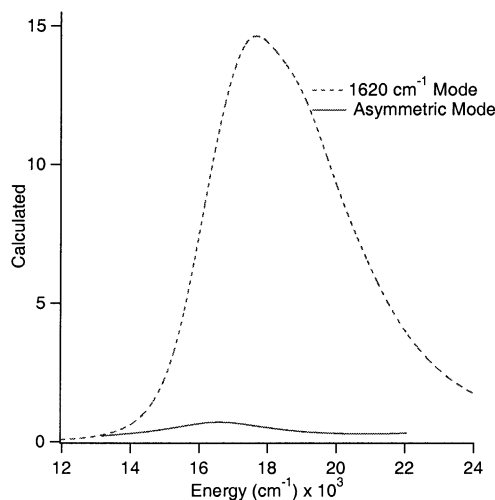
Figure 5. Comparison of Raman intensities for symmetric and asymmetric modes. The dotted line is the calculated resonance Raman profile for the experimentally observed symmetric mode at 1620 cm^{-1}; the solid line is the calculated resonance Raman profile for the 1090 cm^{-1} mode.

The calculated excitation profile for the asymmetric mode that is involved in the intervalence electron transfer is shown in Figure 5. The calculations use the same parameters that define the potential surfaces in Figure 2 and that were used to calculate the absorption spectrum in Figure 3. The calculated profile for the 1620 cm^{-1} symmetric mode, the most intense mode in the experimental spectra, is included in the figure for comparison. The intensity of the asymmetric mode's profile is small but nonzero. The reason can most easily be seen in the strong coupling adiabatic limit. The adiabatic Born−Oppenheimer surfaces in Figure 2 are not displaced relative to each other, the wave packet does not experience a lateral shift, and the time-dependent wave packet in the excited state does not move to overlap with the ground state function. Thus, the resonance Raman intensity is small. However, the two adiabatic surfaces are different from each other because there is a change in force constant in the excited state. Although the wave packet maximum does not shift in the excited state, the ground state function will not be an eigenfunction of the upper surface, and so the wings of the wave packet evolve with time. The intensity caused by this motion is small. The intensity calculated by the exact quantum calculation is approximately 5% that of the 1620 cm^{-1} mode.
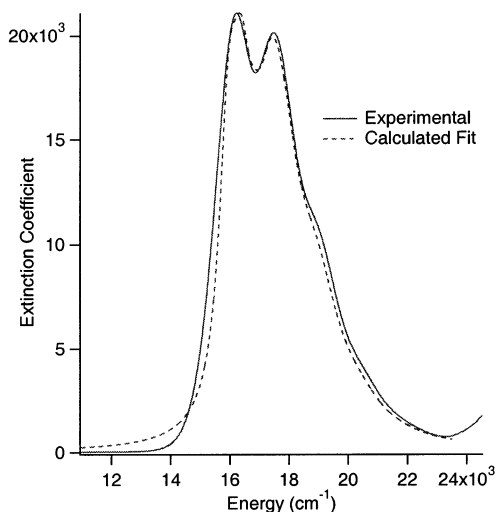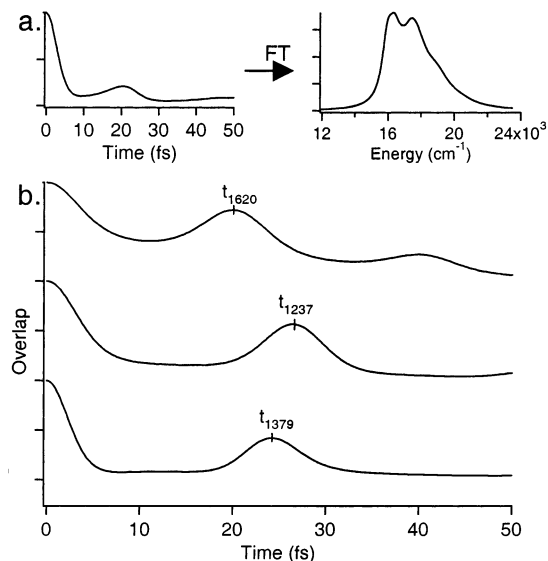
Figure 6. Calculated fit of the absorption spectrum of **(k33)$_2$PD$^+$**; the solid line is the experimental spectrum at room temperature in acetonitrile; the dotted line is the calculated spectrum. Parameters are given in Table 1 for the symmetric modes and section 3 of the Discussion for the asymmetric mode. The electronic origin is determined from the transition in the coupled system. The damping factor, Γ, is 300 cm^{-1}.

There are several other bands observed in the Raman spectra that are enhanced by the amount expected from the calculations and that can be assigned to asymmetric normal coordinates based on the Gaussian electronic structure calculations. Including them in the calculation cannot explain the features of the experimental absorption spectra because the strong coupling always produces narrow absorption bands.

4. Fit of the Electronic Absorption Spectrum. The absorption spectrum of **(k33)$_2$PD$^+$** is calculated by using eq 1, and the parameters are determined from the resonance Raman profiles. The calculated absorption spectrum is shown superimposed on the experimental spectrum in Figure 6. Exactly the same distortions were used to calculate both the absorption spectrum and the Raman profiles that are shown in Figures 4 and 5. The calculated and experimental spectra are all in excellent agreement in all respects including the bandwidths, the band intensities, and the vibronic structure. This quantitative agreement provides a stringent check on the parameters and illustrates the relationship between the two different spectroscopies.

Two aspects of the calculated absorption spectrum require elaboration. First, both the intensities of and the spacings between the vibronic bands are calculated exactly, but there are no normal modes of vibration with exactly the frequency as that observed in the spacings between the bands in the spectrum. This absence of a mode that appears to be required by the vibronic structure is common in the spectra of large molecules in condensed media and is known as the missing mode effect (MIME); its origin is explained in the following section.[36−39] The origin of the MIME in the spectrum of **(k33)$_2$PD$^+$** is also explained in the following section. Second, the presence of the asymmetric mode of Figure 2 has very little effect on the width and structure of the absorption band. The calculated spectrum shown in Figure 6 contains the asymmetric band; the total time-dependent overlap (eq 2) includes the nine symmetric modes and the asymmetric mode. The spectrum calculated without the asymmetric mode is almost identical. The reason is readily explicable in the time domain; the time-dependent overlap involving the asymmetric mode is almost constant, and its

Figure 7. Absolute value of the overlap in the time domain illustrating an MIME; (a) the overlap for the 10 mode calculation and fit of the absorption spectrum and (b) 2 mode pedagogical example of overlap functions for 1620 and 1237 cm^{-1} modes individually and their product resulting in a 1379 cm^{-1} frequency domain progression.

presence or absence does not have a significant effect on the total overlap (the product in eq 2).

5. Vibronic Structure and the Missing Mode Effect (MIME). The absorption spectrum of **(k33)$_2$PD$^+$** contains a regularly spaced vibronic structure with an average energy of 1324 cm^{-1}. The absence of a mode in the resonance Raman vibrational spectrum that appears to be present in the electronic spectrum is called the missing mode effect (MIME).[36−39]

The time-dependent overlap for the 10 modes used in the calculation of the absorption spectrum of **(k33)$_2$PD$^+$** is shown in Figure 7a. The product of the overlaps for all 10 modes used in the calculation gives rise to a single recurrence and is responsible for the spacing in the vibronic structure in the absorption spectrum. It is a consequence of recurrences of all of the modes in the problem but is dominated by the modes with the largest distortions. This is an example of an MIME.

The origin of the MIME can be understood by examining the overlaps in the time domain. The most important characteristic is the recurrence at time t that gives rise to the frequency spacing in the frequency domain at a frequency of $2\pi/ct$. A simple pedagogical example of the effect of two modes is shown in Figure 7b. In this example, the modes at 1620 and 1237 cm^{-1} are chosen. The individual overlaps peak at different times in the time domain (labeled as t_{1620} and t_{1237} in Figure 7b), and the product (eq 2) peaks at an intermediate time (labeled t_{1379}). Therefore, the observed progression has a spacing $\omega_{MIME} = 2\pi/ct_{1379}$ in the frequency domain. Two or more displaced modes can conspire to give a partial recurrence that is not caused by any mode alone. The compromise recurrence is not just the average of t_{1620} and t_{1237}. The MIME frequency may be smaller than any of the individual frequencies, but it is usually between the highest and lowest frequencies and cannot be larger than the highest frequency. The MIME is most clearly interpreted in emission spectra because the vibrational frequencies are those of the ground state for which the frequencies can be measured. In absorption spectra, the vibrational frequencies in the excited

electronic state are relevant and they may differ from those in the ground state.

Each of the displaced modes in the molecule can contribute to the MIME frequency. Each of these modes k has a time dependence whose magnitude is given by eq 8. The larger the displacement Δ, the sharper the peaks in the plot of the overlap of ϕ and $\phi(t)$. The total product overlap will have an MIME closest to $t_k = 2\pi/c\omega_k$ for that mode with the largest Δ_k. A simple formula for estimating the MIME frequency from the displacements has been derived.[36-39]

A requirement for the appearance of the MIME is that the spectrum must not be fully resolved. If the damping is too small, then there will be many recurrences of the overlap in the time domain and the absorption spectrum will exhibit sharp, well-resolved lines. If the damping is too large, then there will be no recurrences of the overlap and the spectrum will consist of only a broad envelope. The emission spectrum of $W(dppe)_2$-$(N_2)_2$ showed how changing the damping by changing the temperature caused the spectrum to change from a series of well-resolved lines to the MIME.[64]

Summary

The transition energy of the intervalence electronic absorption band of the strongly coupled class I **(k33)$_2$PD$^+$** ion can be explained in terms of coupled diabatic potential energy surfaces in an asymmetric normal coordinate with a coupling of 8120 cm^{-1}. This simple model predicts that the spectrum should consist of a single narrow line. The experimental absorption spectrum, however, consists of a broad band with a resolved vibronic structure. The important vibrational normal coordinates that are necessary to understand the spectroscopic properties are investigated by using resonance Raman spectroscopy.

(64) Larson, L. J.; Zink, J. I. *Inorg. Chem.* **1989**, *28*, 3519.

Resonance enhancement provides detailed information about distortions along normal coordinates; the excitation profiles of the **(k33)$_2$PD$^+$** ion reveal that symmetric normal modes are the most highly displaced. The largest distortions are along symmetric carbon–nitrogen and aromatic ring stretching and bending modes. The magnitudes of the displacements are calculated from the integrated intensities in the Raman spectrum. Raman excitation profiles are calculated using a ten-dimensional potential energy surface and the time-dependent theory of spectroscopy. Excellent fits to the profiles are obtained. The asymmetric coordinate gives rise to Raman intensities that are an order of magnitude smaller than those for the displaced symmetric coordinates.

The intervalence absorption spectrum is calculated by using exactly the same ten-dimensional potential surface that was used to calculate the resonance Raman excitation profiles. An excellent fit to both the transition energies and the band shape including the vibronic structure is obtained. The spacing between the vibronic peaks is not the result of a progression in a single normal mode but is an example of the missing mode effect (MIME). The analysis of the class III absorption band using quantitative resonance Raman spectroscopic data illustrates the importance of the symmetric normal vibrational modes in addition to the asymmetric mode that is the usual center of attention.